Materials and Design 30 (2009) 1533–1541

Contents lists available at ScienceDirect

Materials and Design

journal homepage: www.elsevier.com/locate/matdes

Development of novel multilayer materials for impact applications: A combined numerical and experimental approach

A. Tasdemirci [a], I.W. Hall [b,*]

[a] Mechanical Engineering Department, Izmir Institute of Technology, Gulbahce 35437 Koyu, Urla, Izmir, Turkey
[b] Department of Mechanical Engineering, University of Delaware, Newark, DE 19716, USA

ARTICLE INFO

Article history:
Received 5 May 2008
Accepted 30 July 2008
Available online 14 August 2008

Keywords:
Multilayer structures
Numerical simulation
LS-DYNA
Mechanical properties
High strain rate
Stress wave propagation

ABSTRACT

A well-verified and validated numerical model was used to investigate stress wave propagation in a multilayer material subjected to impact loading. The baseline material consisted of a ceramic faceplate and composite backing plate separated by a rubber or teflon foam interlayer: several variants were investigated in which the number, type, and total thicknesses of the interlayers were altered. Comparison of the variants showed that the use of multiple teflon foam interlayers could drastically reduce the average stress in the multilayer material. Based on the numerical results, further experimental work was undertaken upon one of the variants. Very large and unexpected tensile stress oscillations were observed in the ceramic layers, leading to a refinement of the numerical model which successfully reproduced the oscillations and also demonstrated that separation of the sample layers led to trapping of the stress wave within the layers. Use of the validated numerical model allowed detailed analysis of the processes of wave transmission and demonstrates the important synergy that can exist between experimental and modeling studies. The current study provides a valuable starting point for designing future multilayer materials with specific, controlled properties.

1. Introduction

Among many other potential applications, stress wave propagation in multilayer composite materials is relevant to the design and optimization of armor systems for ballistic protection. Layered structures have been a significant contender for developing armor systems and, in many of these, plates of materials with different acoustic impedances are stacked and joined together. The layers typically include materials such as fiber-reinforced composites, ceramics and/or metals. Basically, the aim is to use the ceramic layer to defeat, deform and erode the projectile, and use the composite layer to absorb the remaining energy and increase the fracture and penetration resistance of the armor.

Present multilayer materials have largely been produced from designs based upon experience and intuition but the full potential of future materials can only be efficiently realized through sophisticated modeling and critical experiments. Several studies have modeled penetration into composite materials during high velocity impact [1–6] while other studies have addressed aspects of damage generation [1,7–9]. Work has also been performed to determine loading rate effects: for example, Wu and Chang noted that peak force and energy absorption increased with loading rate as well as noting that fiber breakage caused an increasing amount of energy absorption as the loading rate increased [10]. Also as background to the present study, several authors have studied the penetration of ceramic plates by long-rod projectiles. For example, Anderson and Morris [11] were able to correlate the degree of penetrator erosion with depth of penetration.

Several other reports concern efforts to model the penetration of multilayered materials [12–22]. For example, Espinosa et al. [12] conducted impact recovery experiments on confined multilayered ceramic targets to identify materials and structural design issues to defeat long rod tungsten heavy alloy (WHA) penetrators. They observed that microcracking was the dominant failure mode in multi-layered ceramic targets and attempted to correlate axial stress with crack density. They also studied numerically the response of multilayered ceramic/steel targets to high velocity impact and penetration and they concluded that the penetration process was highly dependent on the multilayered configuration and the target structural design [13]. Gama et al. investigated the through thickness wave propagation and the effect of non-linear material behavior in composite integral armor [14] and also performed a one-dimensional plane strain finite element analysis (FEA) of stress wave propagation to understand the dynamic response and deformation mechanisms of composite structural armor panels [15]. Their studies revealed that armor containing a layer of aluminum foam produced more extensive ceramic fragmentation and less volumetric delamination of the composite backing plate than armor without such a foam interlayer. Ballistic

* Corresponding author. Tel.: +1 302 831 1295; fax: +1 302 831 3619.
E-mail address: halliw@udel.edu (I.W. Hall).

0261-3069/$ - see front matter © 2008 Elsevier Ltd. All rights reserved.
doi:10.1016/j.matdes.2008.07.054

testing of functionally graded materials comprising transitions from a ceramic cermet hard face to a metal back face were studied by Gooch et al. [16]. Gupta demonstrated a concept to enhance the resilience of structures to withstand rapid impulsive loading on multilayered structures [17]. They studied numerically the effects on load spreading of wave speed, layering geometry (thickness and configuration), and mechanical properties (impedance and strength) of the layer and substrate. Mahfuz et al. performed FEA of an integral armor to investigate the response under high-velocity impact and found that, from the delamination point of view, the two interfaces across the rubber interlayer were the most critical [18]. Radin and Goldsmith studied experimentally the response to normal impact of hard-steel blunt and conically-nosed projectiles on multi-layered plates of soft aluminum, both adjacent and spaced, as well as on adjacent disks of thin aluminum and polycarbonate, including sandwich arrangements [19]. It was found that the ballistic resistance of a monolithic metallic target was greater than that of several adjoining plates of the same thickness.

Robbins et al. [20] examined the effects of layer damage and imperfect interfaces on load spreading and projectile defeat capabilities of the multilayered targets and concluded that high impedance and strength of the layers enhanced the projectile defeat capability of the target. The study by Roeder and Sun of the effects of structural layering and thermal residual stresses on impact resistance of alumina/aluminum laminated structures showed that thick layer laminates allowed less penetration than thin layer laminates. Yadav and Ravichandran [23] performed ballistic penetration experiments on ceramic tiles laminated with thin layers of polymer in between. Their results demonstrated that penetration resistance of an unconfined ceramic structure can be improved significantly by laminating ceramic tiles with thin polymer layers in between.

However, these earlier studies are exceedingly difficult to validate directly and do not address the details of the early stages of the impact phenomenon, particularly events occurring at a microstructural level and within the first few microseconds after impact. Understanding the behavior of the material during the first few reverberations may be critical to designing better multilayer materials and previous studies [23–27] by the present authors have provided the first precise theoretical and experimental insights into the details of stress wave propagation in these materials.

The approach was to use the split Hopkinson pressure bar, not as a device for generating mechanical property data, but as a probe for generating entry and exit waves of known characteristics. These known, measured, entry and exit waves were then reproduced in a finite element model of the multilayer material. It was confirmed that when the model data matched the output data from the bars, the model was accurately describing the stress-state within the multilayer material [28]. To date it has been possible to accurately reproduce data from a wide variety of single, double and triple-layered materials. By steadily increasing the incident stress wave amplitude the material models have been gradually developed so as to incorporate elasticity, hyper-elasticity, plasticity, certain types of damage, and some cases of fracture.

Once a model has been satisfactorily validated, it becomes possible to re-construct the entire history of the sample microsecond by microsecond. For example, stress/distance/time plots can indicate the level of any of the stresses at any point within the test specimen as a function of time. Also, it becomes possible to use the model in a predictive capacity, e.g. to conduct parametric studies involving changing important variables such as layer thickness, the number of interlayer and their locations.

The objective of this work was to demonstrate that it is possible to facilitate the material design process by identifying and testing only those configurations which hold promise for significant performance improvement: it is intended to guide the testing program, not do away with it entirely. The primary thrust of the present work was, therefore, to use the well-verified and validated numerical model to demonstrate the effect on stress wave propagation of varying the number and thicknesses of the interlayers in the multi-layer composite materials. What emerged, however, was not only a deeper understanding of the processes of wave propagation in these materials but also confirmation of the importance of performing critical experiments to guide further model development.

2. Modeling

A three-dimensional SHPB finite element model was used to study stress wave propagation in the multi-layer materials and also in the individual components. The model captures details of wave scattering, transmission and reflection at the interfaces between layers for the material combinations investigated at intervals of 1 μs. The analysis was performed using the commercial explicit finite element code LS-DYNA 971. Model and mesh were generated in LS-INGRID. Two axes of symmetry were assumed so only one quarter of the bar was modeled in the SHPB model. For each SHPB test specimens modeled, the output was displayed at several locations within the sample as well as at the location of the strain gages on the incident and transmitter bars of the SHPB apparatus. Ideally, the output calculated by the model from the bars and the sample closely matches the data actually measured by strain gages on the incident and transmitter bars and sample: this then indicates that the model is accurately capturing the wave propagation behavior in the sample and bars. The model can then be used with confidence to determine local conditions at any point within the sample: this information can be used, for example, to predict fracture initiation sites, local stress gradients and discontinuities. Data selected for presentation in the figures below are z-stress levels taken from the center-line of the samples rather than from the surface locations used for model verification.

The SHPB model had four components in contact; a striker bar of length 356 mm, an incident bar and a transmission bar each of length 1524 mm, and the specimen. In order to maintain continuity with earlier experimental work, the materials used in these multilayer composites were ceramic, EPDM rubber or teflon foam (*Polarchip™)[1] and S2–Glass/SC15 composite. Further details of the mechanical properties of the materials and the material models used in the finite element models can be found in [25]. The bar diameter was 19.05 mm and the elastic wave velocity was 5003 m/s. Initially, specimens were subjected to circumferential constraint since earlier work had shown this to be important in influencing the actual behavior of the material. Specifically, lack of constraint allows free lateral expansion of the low modulus interlayers and delays wave transmission while the presence of constraint highlights the effect of Poisson's ratio on the wave transmission behavior as explained further below.

The finite element grid of the quarter section of the bars and finite element mesh of the SHPB model are shown in Fig. 1. A total of 75 elements were used in the model for the cross-section, which provided 10 elements across the radius of the bars. 400 elements were used along the length of the bar. Mesh biasing along the bar axis was utilized to refine the meshes at the contact interfaces. The mesh sensitivity of the Hopkinson bar model under a known stress pulse in the axial direction (*z*-direction) was investigated by varying the number of elements along the length of the bars and the specimen, while varying the number of elements in the cross-section of the specimen and the bars. Calculations were performed for several different mesh densities in order to check for mesh sensitivity. It was observed that the axial stress contained

[1] *Polarchip™ is a trademark of W. L. Gore, Inc.

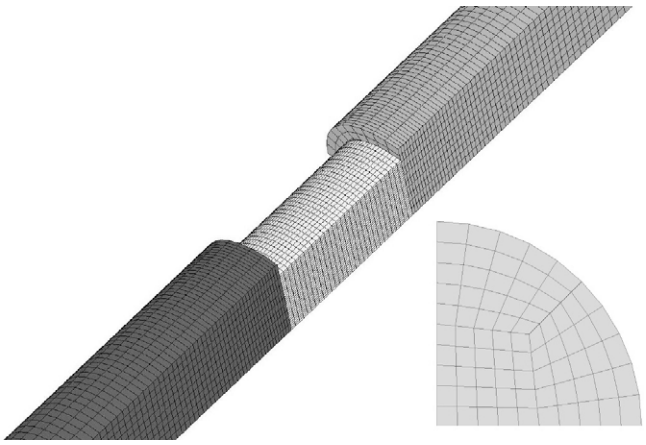

Fig. 1. Finite element mesh used in the model of SHPB and elements used in the bar cross-section.

oscillations of the same frequency as those that are experimentally observed in finite diameter bars, and which are known as Pochhammer modes. The ability to accurately reproduce these stress oscillations confirmed that mesh sensitivity was not a problem. Based on these trials, the acceptable minimum numbers of elements were defined and the meshes consisting of these elements were used throughout the study.

Material properties used in the simulation are given in Table 1. Ceramic layers were modeled with an isotropic elastic material model and composite layers were modeled with an orthotropic elastic material model. Since rubber and expanded teflon are significantly nonlinear elastic materials their behavior was studied by modeling them with experimentally determined data. Rubber was modeled with the Ogden material model and is considered to be fully incompressible, since its bulk modulus greatly exceeds the shear modulus in magnitude. To model the rubber as an unconstrained material, a hydrostatic work term is included in the strain energy functional, which is a function of the relative volume. In the Ogden material model, the strain energy density can be expressed in terms of the principal stretches λ_α, $\alpha = 1,2,3$ as:

$$W(\lambda_1,\lambda_2,\lambda_3) = \sum_{p=1}^{N} \frac{\mu_p}{\alpha_p}(\lambda_1^{\alpha_p} + \lambda_2^{\alpha_p} + \lambda_3^{\alpha_p} - 3)$$

where N, μ_p and α_p are material constants. Under the assumption of incompressibility it can be rewritten as

$$W(\lambda_1,\lambda_2) = \sum_{p=1}^{N} \frac{\mu_p}{\alpha_p}(\lambda_1^{\alpha_p} + \lambda_2^{\alpha_p} + \lambda_1^{\alpha_p}\cdot\lambda_2^{\alpha_p} - 3)$$

In general the shear modulus results from

$$2\mu = \sum_{p=1}^{N} \mu_p \cdot \alpha_p$$

Table 1
Material properties used in finite element models

Material	Modulus of elasticity (GPa)	Poisson's ratio	Density (kg/m^3)	Other
Ceramic	370	0.22	3900	–
Rubber	–	0.4995	1200	$\mu_1 = -4.684$ (MPa), $\alpha_1 = -1.856$ $\mu_2 = 0.1954$ (MPa), $\alpha_2 = 2.992$
Teflon	3.65	0.25	760	–
Composite	E_1: 27.5	v_{21}: 0.12	1850	G_1: 2.9 (GPa)
	E_2: 27.5	v_{31}: 0.173		G_2: 2.14 (GPa)
	E_3: 27.5	v_{32}: 0.173		G_3: 2.14 (GPa)
Inconel	207	0.3	7850	–

with $N = 3$ and by fitting the material properties, the material behavior of EPDM can be described accurately. For particular values of material constants, the Ogden model will reduce to either the Neo–Hookean solid ($N = 1$, $\alpha = 2$) or the Mooney–Rivlin material ($N = 2, \alpha_1 = 2, \alpha_2 = -2$).

Using the Ogden material model, the three principal values of the Cauchy stresses can now be computed as

$$\sigma_\alpha = p + \lambda_\alpha \frac{\partial W}{\partial \lambda_\alpha}.$$

The material model gives good correlation with the test data in simple tension up to strains of 700%. Expanded teflon is modeled with the crushable foam model and this material model is dedicated to modeling crushable foam with optional damping and tension cut-off. Unloading is fully elastic. Tension is treated as elastic–perfectly plastic at the tension cut-off value. There is also a failure stress of 50 MPa which was adjusted by trial and error to give best possible agreement with the Split Hopkinson Pressure Bar results and to keep the deformation of the layer within the reasonable values. For determining the constants of the Ogden and crushable foam models, the stress vs. strain curve is used as an input and the least square fit to the experimental data is performed during the initialization phase.

The component materials were modeled with eight nodes solid elements and the interfaces were modeled with the automatic contact sliding interfaces without friction. The impact velocity of the striker bar had been defined as the initial condition and all other boundaries were traction free and could move in any direction. In order to save computation time, the simulation used bars 1524 mm in length instead of full length bars. It is noted that this has the effect of decreasing the transit time between successive waves and shortening the wave duration slightly: however, it does not affect the basic wave-shapes or amplitudes. A few trial computations were carried out using full-length bars but, apart from the slightly smaller time window, no significant differences were found and the shorter bars were used henceforth. The accuracy of the numerical model was verified by simulating the one-dimensional stress wave propagation in a long rod with free and fixed end conditions. The contact definitions between bar-specimen and bar–bar interfaces were cross-checked by computing the reflection coefficients from an interface with unequal cross-sections. The impact-contact definition of a striker bar on the incident bar was verified by computing the stress in the bar. The model was found to predict all the above-mentioned analytical problems with sufficient accuracy. This well-verified and validated model was used in the present study.

For time step calculation, the automatic time step calculation option was chosen. In this option LS-DYNA determines the initial time step size. During the solution LS-DYNA loops through the elements and determines a new step size by taking the minimum value over all elements.

$$\Delta t^{n+1} = \mathrm{TSSFAC}^* \min\{\Delta t_1, \Delta t_2 \ldots \Delta t_N\}$$

where N and TSSFAC are the number of elements and scale factor for computed time step, respectively. The time step size roughly corresponds to the transit time of an acoustic wave through an element using the shortest characteristic distance. For stability reasons the scale factor TSSFAC was set to a value of 0.90. Again, the ability to reproduce Pochhammer–Chree oscillations confirmed that the time steps were small enough to capture all necessary details of the wave propagation.

In the actual split Hopkinson experiment, the measured quantities are the impact velocity of the striker bar, and strain values on the incident and transmitter bar surfaces as a function of time measured via strain gages mounted on the bar surfaces. In the numerical simulation, displacement and velocity of nodes, strain

and stress of the elements, interface forces, material and global energies can all be obtained from the code. Time history data of the nodal, element and interface data are also available. The model is potentially, therefore, a very powerful tool to understand the processes of wave propagation in multilayer materials.

By using the results of numerical modeling it was possible to construct stress/distance/time plots to indicate the stress level at any point within the test specimen as a function of time as well as to conduct parametric studies involving changing the number, order and relative thicknesses of the layers. It is known that the location of the interlayer has an important influence on the stress wave propagation behavior of multilayer systems [25]. In order to keep all parameters constant as far as possible, the numerical results presented in this paper were carried out at an incident bar velocity of 20.5 m/s and, except where specified, for the configuration with constrained interlayers.

3. Results

3.1. Numerical modeling

Apart from the baseline configuration, which has an interlayer between the ceramic and composite components, the four different geometric variants shown in Fig. 2 were analyzed for this purpose. For the first variant, instead of having an interlayer between the ceramic and composite components, the interlayer was carried to the mid-length of the ceramic component. For the second variant, this interlayer was carried to the mid-length of the composite component. For the third variant, two separate interlayers were placed: the first one was at the ceramic mid-length and the second at the ceramic–composite interface. For the fourth variant, three separate interlayers were placed. The first two were at the same locations as for the previous variant and the third one was at the mid-length of the composite. The interlayer consisted of either a 1.5 mm thick layer of ethylene propylene diene monomer (EPDM) rubber or expanded teflon foam. Results for the baseline configuration (interlayer between the ceramic and composite) will also be briefly represented here to clarify the effect of adding new layers and changing their locations.

In the following simulations, radial expansion of the interlayers has been prevented since prior experimental and numerical results had shown that constraining the rubber interlayer in this fashion imposed a type of worst-case scenario on the system. Without constraint, the rubber was free to expand laterally and a significant delay occurred before the initial stress rise because of the large acoustic impedance mismatches between the components. However, when constrained, the rubber became rigid almost instantaneously and the stress rose almost instantaneously as well since the acoustic mismatch between ceramic, rubber and composite diminished greatly and facilitated passage of the stress waves. Although the simulations include constraint, prior results showed that constraint of the teflon foam interlayer has negligible effect since the foam compresses dramatically and has an essentially zero Poisson's ratio: consequently, constrained and unconstrained teflon-containing samples behave very similarly.

From the point of view of designing armor, therefore, interest in the following simulations centers on both delaying and attenuating the stress waves.

3.1.1. Baseline configuration

Fig. 3a and b shows the evolution with time of the z-stress at the centerline of specimens with rubber and teflon, respectively, as a function of normalized sample length for the baseline configuration. The 'time window' for the test, i.e., the interval during which the wave is passing through, is about 190 μs; this is represented by the vertical width of the central horizontal region of the figures. It

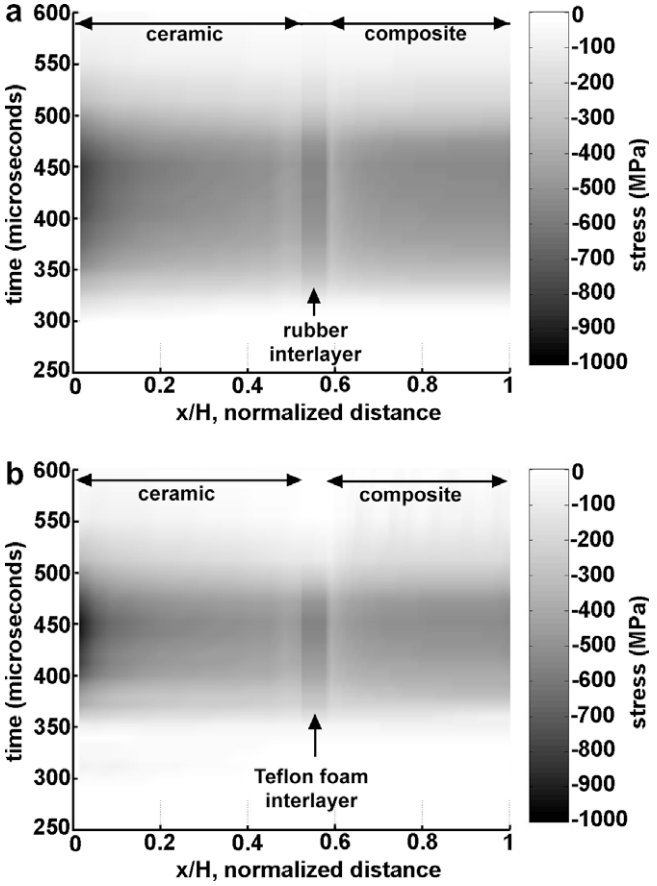

Fig. 3. Z-stress/time/distance maps showing response of baseline configuration 3-layer sample with different interlayer materials: (a) rubber, and (b) teflon foam.

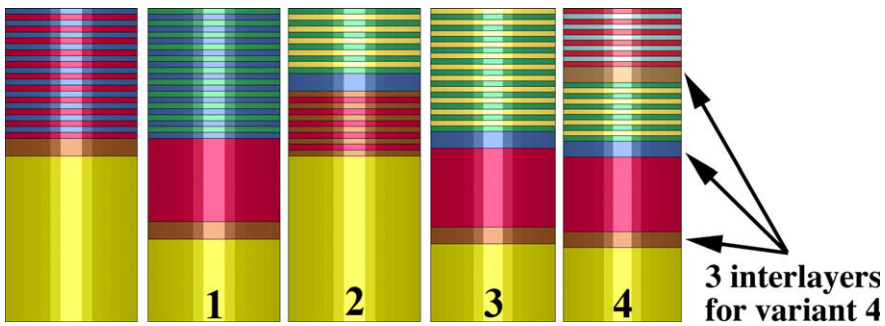

Fig. 2. Baseline configuration and different variants of interlayer configurations used in the finite element study: the three interlayers present in variant 4 are indicated.

is clear that, during high strain rate compression loading of this multilayer material, the z-stress within the specimen was never uniform. The present results showed that using a rubber interlayer was causing more non-uniform stress distribution particularly inside the ceramic layer than that of the teflon containing specimen. The presence of the teflon interlayer actually gave rise to a narrower stress pulse inside the material (i.e., the vertical width of the main feature of the figure) by causing a stress-rise delay about 50 μs.

Parametric studies involving changing the location and the number of interlayers were now undertaken.

3.1.2. Variant 1

As a first example, we consider moving the location of the interlayer to the mid-length of the ceramic. Total ceramic thickness was kept constant; the interlayer was placed at the mid-length of the ceramic layer. Fig. 4a and b shows the evolution with time of the z-stress at the centerline of the sample as a function of normalized sample length for rubber and teflon, respectively. It is seen that moving the interlayer from the ceramic–composite interface in the first variant led to a drastically increased stress discontinuity at the ceramic–composite interface (indicated by the dark region) and caused a highly non-uniform stress distribution inside the ceramic layer.

Fig. 5 is a section through the z-stress/time/distance plots and shows quantitatively the variation of z-stress with position along the central axis of the samples at 450 μs after the beginning of the test for the baseline configuration and first variant. The increased severity of the stress gradients in ceramic and composite

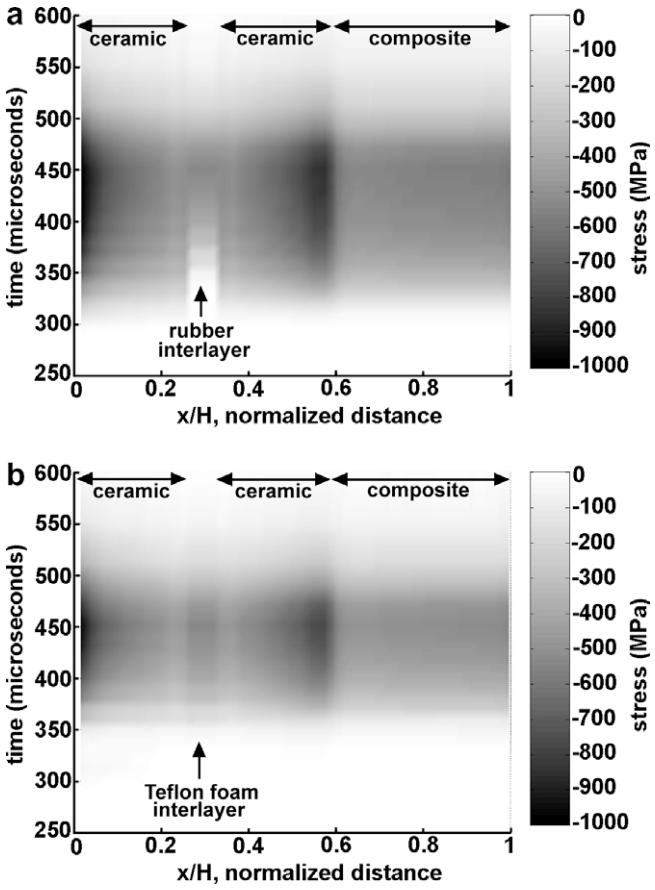

Fig. 4. Z-stress/time/distance maps showing response of the first variant 3-layer sample with different interlayer materials: (a) rubber, and (b) teflon.

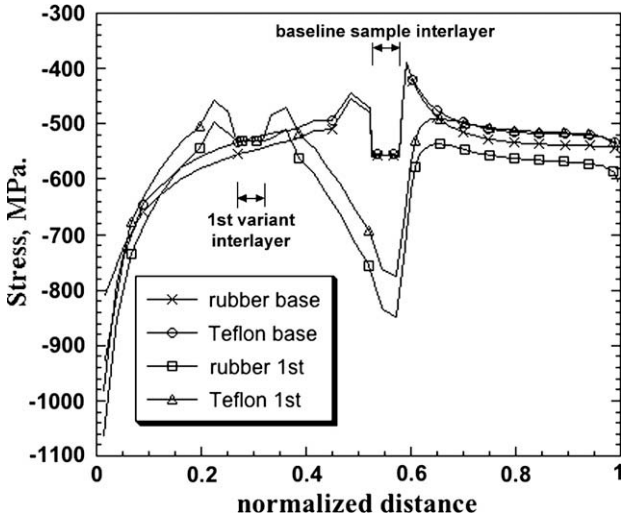

Fig. 5. Stress vs. position within sample for teflon and rubber interlayer at 450 μs into the test for the baseline and first variant.

for variant 1 in the region of their interface is now clearly visible. Nevertheless, by comparison, the teflon interlayer led to slightly lower stress values in this region.

3.1.3. Variant 2

For the second variant, the interlayer was positioned at the half-length of the composite component: the total composite component thickness was again kept constant. Fig. 6 shows stress vs. position within samples containing rubber and teflon foam interlayers at 450 μs for the baseline configuration and second variant. When compared with the baseline configuration, the ceramic experienced a significantly more non-uniform stress distribution. The stress discontinuity at the ceramic–composite interface was much greater than at the corresponding location in the baseline configuration and there was a significant stress discontinuity between the composite layers.

3.1.4. Variant 3

Fig. 7a and b shows the evolution with time of the z-stress at the centerline of the sample as a function of normalized sample length

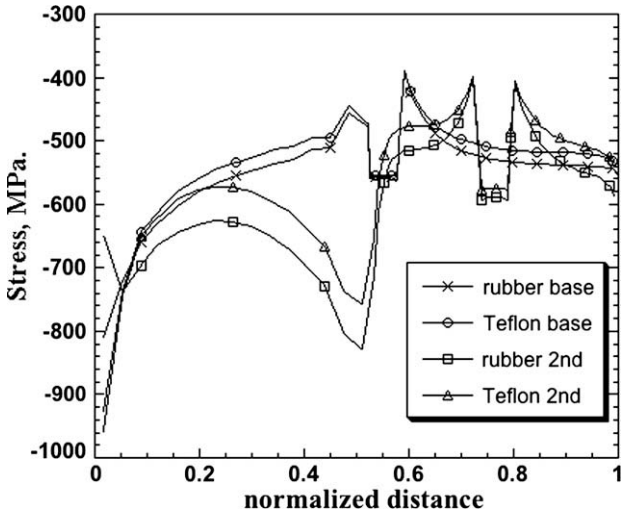

Fig. 6. Z-stress vs. position within sample for teflon and rubber interlayer at 450 μs into the test for the baseline configuration and second variant.

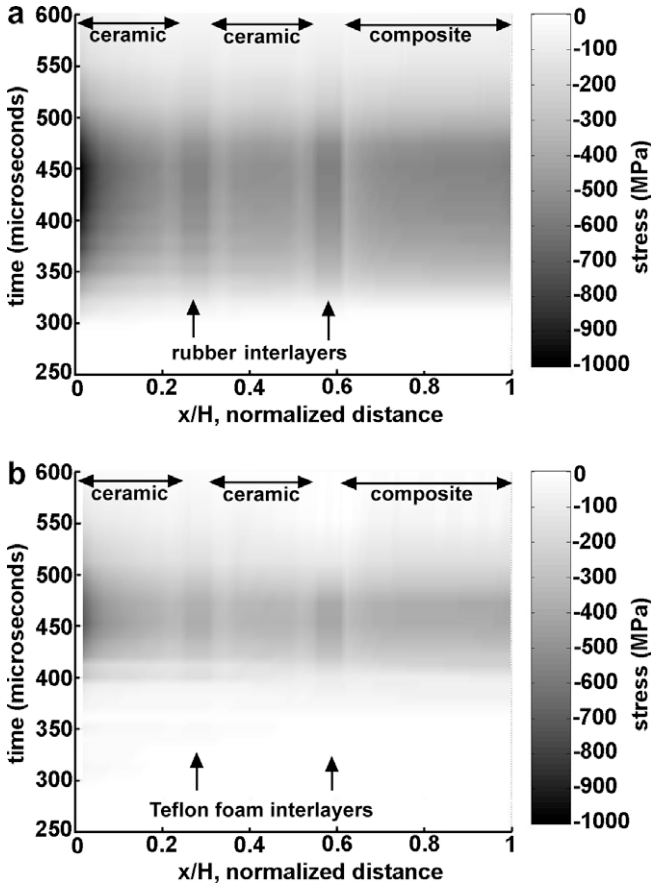

Fig. 7. Z-stress/time/distance maps showing response of the third variant 5-layer sample with different interlayer materials: (a) rubber, and (b) teflon.

for the third variant. There are now five separate layers in this variant. Note that the time window during which the stress is around its maximum level (i.e., the dense grey bands of Fig. 7a and b) is much shorter for the sample with teflon foam interlayers.

Fig. 8 shows that in this third variant with the Teflon interlayer the average stress (i.e., averaged over the entire length of the sample) was ~350 MPa whereas in the baseline configuration counterpart the average stress was ~500 MPa. In addition, use of the Teflon foam in this new configuration caused a stress-rise delay of ~100 μs. With rubber interlayers, stress values in regions close to the front surface of the ceramic layer were lowered somewhat but the average stress through the thickness did not change as significantly as for the case with the Teflon interlayer.

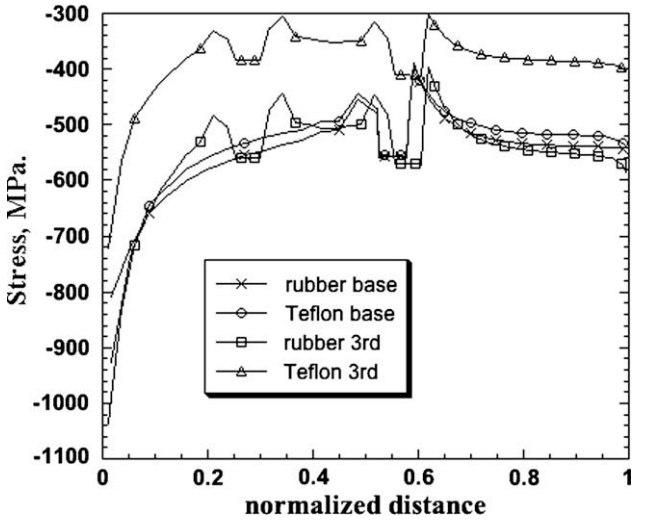

Fig. 8. Z-stress vs. position within sample for teflon and rubber interlayer at 450 μs into the test for the baseline configuration and third variant.

3.1.5. Variant 4

A similar set of simulations was then carried out for the fourth variant which now contained seven separate layers. Fig. 9a and b shows the evolution with time of the z-stress at the centerline of the sample as a function of normalized sample length for the fourth configuration. Major differences are now seen between the behaviors of different configurations. In comparison with the baseline configuration, the teflon-containing fourth variant gave rise to a stress wave of drastically reduced amplitude and significantly reduced wavelength. Also noteworthy is the fact that the time delay for the stress wave to build up was now maximized: in fact the build-up did not occur until about 440 μs into the test which is significantly greater than for any of the prior cases. Fig. 10 shows that the average stress experienced in samples with the fourth configuration was 200 MPa compared with 550 MPa for the baseline configuration.

3.2. Experimental

Since the modeling described above had identified specific architectures as particularly noteworthy in terms of (a) reducing the average stress within the sample and (b) delaying the stress

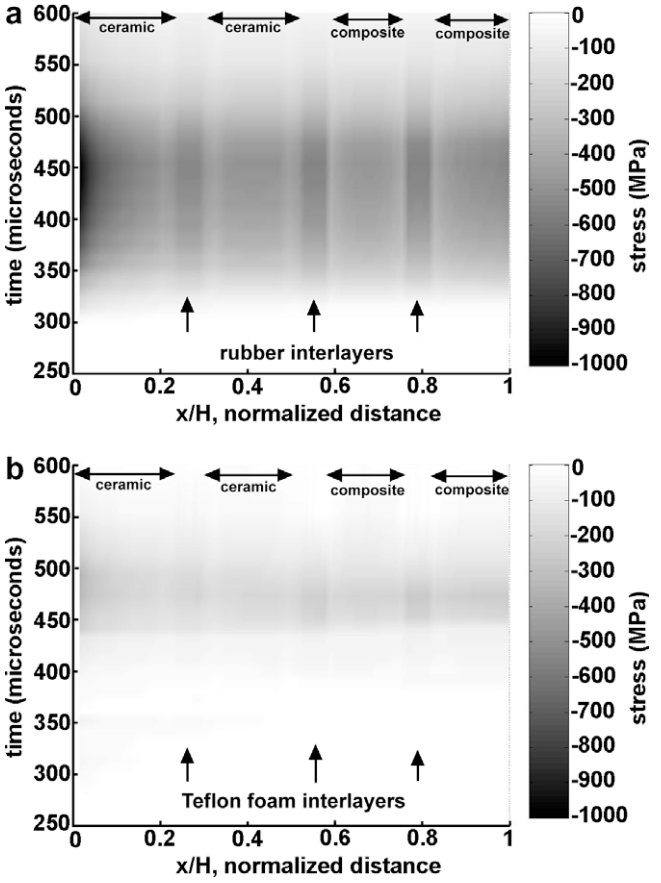

Fig. 9. Z-stress/time/distance maps showing response of the fourth variant 7-layer sample with different interlayer materials: (a) rubber, and (b) teflon.

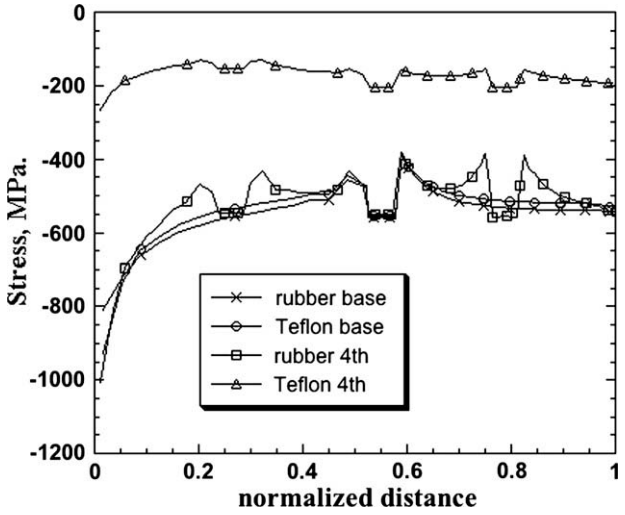

Fig. 10. Z-stress vs. position within sample for teflon and rubber interlayer at 450 μs into the test for the baseline configuration and fourth variant.

rise, experiments were carried out to corroborate the numerical results. Samples of variant 3 were prepared and the ceramic and composite layers were strain gauged, Fig. 11.

Fig. 12 shows measured data from the incident + reflected wave and transmitted wave in the SHPB apparatus for two samples, one is the baseline configuration and the other is variant 3. The long delay in the rise time for the stress in variant 3 is indicated by Δt, during which time almost none of the wave passes into the composite layer but is instead either being reflected directly back into the incident bar or is 'trapped' in the ceramic layers. Note also that when the transmitted wave for the sample with 2 teflon interlayers does begin to develop, its amplitude is greatly reduced compared with that of the baseline configuration.

The sample behavior was found to be considerably more complex than suspected from the model, particularly at longer times, i.e., outside the initial ~190 μs window normally investigated. For example, in samples with teflon foam interlayers, strain gage data revealed that the ceramic layers suffered initial compressive stress followed almost at once by rapid oscillations that included severe tensile stresses, Fig. 13a. The existence of severe tensile stresses was borne out by the observation that, in each of the three tests carried out, the first ceramic layer fractured into several pieces.

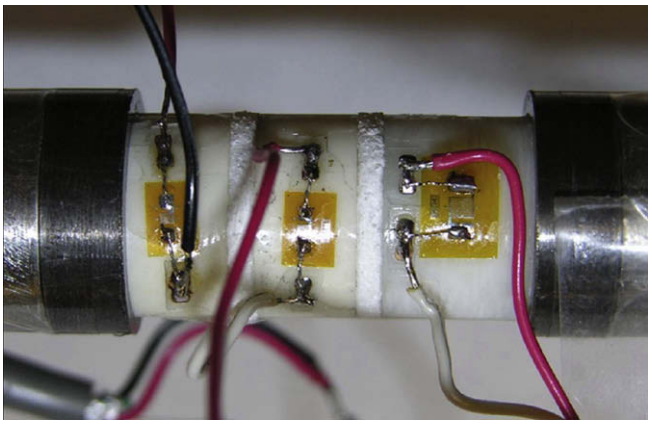

Fig. 11. Variant 3 sample with teflon foam interlayers, strain gauged and ready for testing.

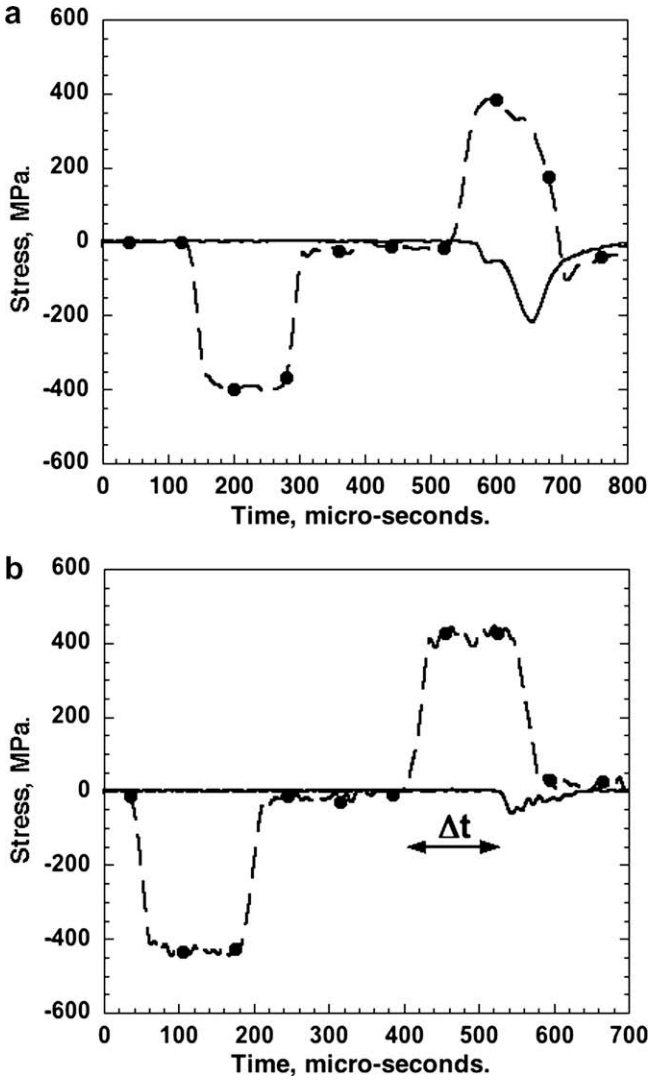

Fig. 12. Experimentally measured SHPB data for samples (a) with a single Teflon foam interlayer, and (b) three teflon foam interlayers.

With the extra information concerning stress oscillations provided by these tests, the model was further examined to see whether these characteristics could be reproduced in the model and also to examine the behavior at longer times. Very similar stress oscillations could be reproduced in the model by eroding elements in the interlayer, as justified below, as soon as the maximum principal stress there reached 50 MPa, Fig. 13b. A perfect match is not possible since the actual shape of the oscillations was found to be extremely sensitive to position within and on the surface of the sample; Fig. 13c shows the locations of the nodes used for the construction of Fig. 13b. It should be pointed out that the resolution of the model is potentially superior to that of the strain gages which effectively 'average out' the data from an area of approximately 1.5 mm^2, i.e., considerably larger than that represented by one of the model nodes. The model also indicated that erosion of the foam interlayers led to complete separation of the three major layers from each other at later stages of the test, Fig. 13c. Complete erosion of the interlayer is justified since observations by high-speed photography indicate that, in three-layer specimens, the Teflon foam interlayer is essentially pulverized and ejected during the impact event, Fig. 14a and b at very low stresses.

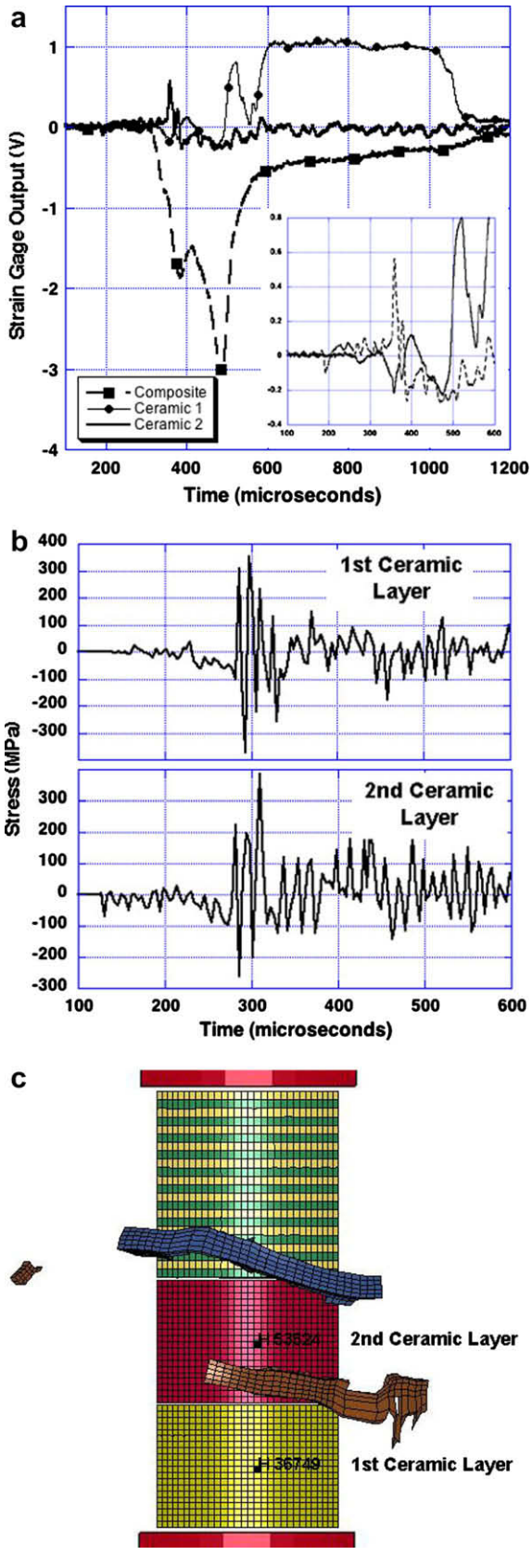

Fig. 13. (a) Experimentally measured stress oscillations in the three layers of a variant 3 sample: the inset shows the early oscillations in the ceramic layers in greater detail: (b) stress oscillations in the first and second ceramic layers generated by the numerical model: (c) detail of the numerical model at 700 μs: close examination shows that erosion of the teflon foam causes separation of the three layers and total lack of contact between them and the ends of the Hopkinson bars.

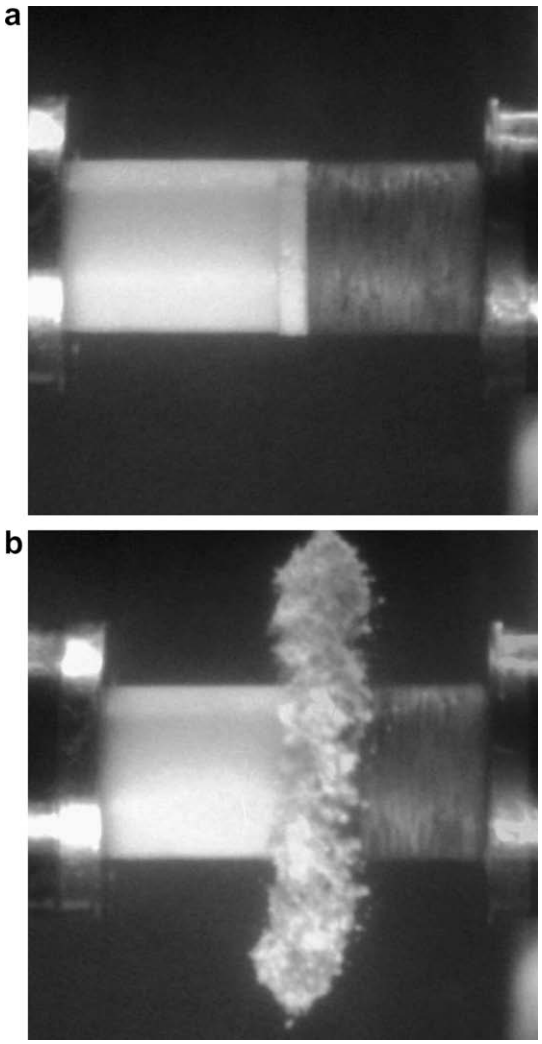

Fig. 14. High-speed photography of experiment with ceramic/unconstrained teflon foam/composite sample: (a) before impact, and (b) showing pulverization and ejection of teflon foam debris shortly after impact.

4. Discussion

Prior studies had shown that it is possible to accurately reproduce data from a variety of single, double and triple layered materials. The motivation for the present work, therefore, was to use the well-verified and validated numerical model to demonstrate its potential in aiding the design of improved multilayer materials without the need for repetitive experimental tests. This was achieved here by studying the effect of varying the number and thicknesses of the interlayers on stress wave propagation in the multilayer composite materials.

Numerical calculations confirm that the differences in calculated stress-distance time maps are related to the number and thicknesses of the interlayers and the mechanical properties of the interlayer materials. Comparison of Figs. 3 and 4 shows that moving the interlayer to the centre of the ceramic had little effect in preventing stress rise in the ceramic. Neither of these first variants seemed, therefore, to be better than the baseline configuration: on the contrary, two regions of severe stress discontinuity occurred as can be noted in Fig. 4. These will lead to significant local stress/strain gradients and could increase the tendency to brittle fracture. The increased stress concentration seen in the ceramic for variant 1 is very undesirable as it can lead to fracture initiation.

The teflon foam began to show its effectiveness in reducing the overall stress value in the composite layer in variant 2 and this effectiveness became much more apparent in the 3rd and 4th variants. Not only was the stress distribution now more uniform but also a significant stress rise delay occurred inside the layers as compared to the 1st and 2nd variants.

In terms of damage to the composite, it may be anticipated that damage to the composite backing plate should be reduced for the third and fourth variants, relative to the baseline configuration since the average stress has been significantly reduced. A major reason for the predicted decrease in the stress level is because of geometric attenuation, where some of the reflected waves are cancelled by interference with incoming waves in individual layers. The necessary strong reflections occur because the teflon foam has an exceptionally small Poisson's ratio and, since there was little radial expansion, radial constraint had little effect on the axial properties. The axial modulus, therefore, remained low and the acoustic impedance mismatch between the two pairs of components remained high throughout the period where the Teflon was being compressed axially. Consequently, much of the energy of the wave is dissipated in the ceramic layers, and the occurrence of the observed tensile stress oscillations even leads to fracture of the first layer. This may be compared with the behavior of a constrained rubber interlayer where the modulus increases rapidly and extensive destructive interference between incoming and reflected waves is not possible so that the wave passes directly into the composite backing layer.

The response of multilayer materials to the propagation of stress waves is an exceptionally complex function of many variables and can only be effectively addressed through a combination of 3D modeling and parallel testing rather than either one alone. The synergy between the two tools is especially evident in the present work since the existence of tensile stresses in the ceramic layers of variant 3 was first detected experimentally through the use of strain gauged samples. Thereafter, when the model was refined and examined, similar tensile reflections were observed and the model now revealed further behavior that was neither available nor suspected from the experimental study, namely that the ceramic layers became effectively separated from each other and from the composite during later stages of the testing and that this led to trapping of the wave within the layers. This process of trapping undoubtedly contributes to the reduction of stress measured in the composite layer.

5. Conclusions

The use of a validated numerical model allowed detailed analysis of the processes of stress wave transmission and these parametric studies provide a useful starting point for designing future multilayer materials with specific, controlled properties. The present study showed that the lowest stresses were found in the 4th variant indicating that, for these pulses of limited duration, this configuration provides better protection for the ceramic and composite backing plate than the baseline configuration.

Unexpectedly large tensile stresses were detected experimentally in the ceramic layers and subsequently confirmed numerically.

Of course, a multitude of other considerations, such as cost, manufacturability, areal weight, etc., must also be taken into account; nevertheless, it is clear that such modeling can guide the design and development of future multilayer materials. Further developments which are under way include the extension of the current work to a design optimization study in which the optimum thicknesses of the each layer are determined. In principle, therefore, it will be possible to geometrically tailor a multilayered material system in which the minimum stress experienced in the backing plate can be specified for any impact velocity.

Acknowledgements

The authors gratefully acknowledge financial assistance during the course of this research from the Army Research Office, Solid Mechanics Branch, Dr. B. LaMattina Program Manager, and NSF Award #0242772, Office of International Science and Engineering Dr. O. Shinaishin, Program Manager. The authors also thank Drs. J. Gillespie and B.A. Gama, Center for Composite Materials, University of Delaware, for some of the three-layer composites and W.L. Gore and Associates Inc for provision of the teflon foam (Polarchip™) interlayers.

References

[1] Chen JK, Allahdadi FA, Carney TC. High-velocity impact of graphite/epoxy composite laminates. Compos Sci Technol 1997;57(9–10):1369–79.
[2] Lee SWR, Sun CT. Dynamic penetration of graphite–epoxy laminates impacted by a blunt-ended projectile. Compos Sci Technol 1993;49(4):369–80.
[3] van Hoof J, Worswick MJ, Williams K. Backplane response of ballistically impacted composites. J De Phys Iv 2000;10(P9):659–64.
[4] Papanicolaou GC et al. Impact damage and residual strength of FRP composites. In: Impact response and dynamic failure of composites and laminate materials, Pts 1 and 2; 1998. p. 127–47.
[5] Yen CF. Ballistic impact modeling of composite materials. Dearborn, Michigan: Livermore Software Technology Corporation (LSTC) and Engineering Technology Associates, Inc. (ETA); 2002.
[6] Wen HM. Penetration and perforation of thick FRP laminates. Compos Sci Technol 2001;61(8):1163–72.
[7] Goldsmith W, Dharan CKH, Chang H. Quasi-static and ballistic perforation of carbon-fiber laminates. Int J Solids Struct 1995;32(1):89–103.
[8] Hsiao HM, Daniel IM, Cordes RD. Dynamic compressive behavior of thick composite materials. Exp Mech 1998;38(3):172–80.
[9] Kumar KS, Bhat TB. Response of composite laminates on impact of high velocity projectiles. In: Impact response and dynamic failure of composites and laminate materials, Pts 1 and 2; 1998. p. 337–48.
[10] Wu E, Chang LC. Loading rate effect on woven glass laminated plates by penetration force. J Compos Mater 1998;32(8):702–21.
[11] Anderson CE, Morris BL. The ballistic performance of confined Al_2O_3 ceramic tiles. Int J Impact Eng 1992;12(2):167–87.
[12] Espinosa HD et al. Enhanced ballistic performance of confined multi-layered ceramic targets against long rod penetrators through interface defeat. Int J Solids Struct 2000;37(36):4893–913.
[13] Espinosa HD et al. A numerical investigation of penetration in multilayered material/structure systems. Int J Solids Struct 1998;35(22):2975–3001.
[14] Gama BA, Gillespie Jr JW, Bogetti TA, Fink B. Innovative design and ballistic performance of lightweight composite integral armor. In: SAE 2001 World Congress. Detroit, MI: SAE; 2001.
[15] Gama BA et al. Aluminum foam integral armor: a new dimension in armor design. Compos Struct 2001;52(3–4):381–95.
[16] Gooch WAC, Burkins BHC, Palicka MS, Rubin R, Ravichandran J. Development and ballistic testing of a functionally gradient ceramic/metal applique. Mater Sci Forum 1999;308–311:614–21.
[17] Gupta YM, Ding JL. Impact load spreading in layered materials and structures: concept and quantitative measure. Int J Impact Eng 2002;27(3):277–91.
[18] Mahfuz H et al. Investigation of high-velocity impact on integral armor using finite element method. Int J Impact Eng 2000;24(2):203–17.
[19] Radin J, Goldsmith W. Normal projectile penetration and perforation of layered targets. Int J Impact Eng 1988;7(2):229–59.
[20] Robbins JR, Ding JL, Gupta YM. Load spreading and penetration resistance of layered structures – a numerical study. Int J Impact Eng 2004;30(6):593–615.
[21] Roeder BA, Sun CT. Dynamic penetration of alumina/aluminum laminates: experiments and modeling. Int J Impact Eng 2001;25(2):169–85.
[22] Yadav S, Ravichandran G. Penetration resistance of laminated ceramic/polymer structures. Int J Impact Eng 2003;28(5):557–74.
[23] Tasdemirci A. Experimental and modeling studies of stress wave propagation in multilayer composite materials. In: PhD thesis, mechanical engineering, University of Delaware: Newark, DE; 2005. p. 240.
[24] Tasdemirci A, Hall IW. Numerical and experimental studies of damage generation in multi-layer composite materials at high strain rates. Int J Impact Eng 2007;34(2):189–204.
[25] Tasdemirci A, Hall IW. Experimental and modeling studies of stress wave propagation in multilayer composite materials: low modulus interlayer effects. J Compos Mater 2005;39(11):981–1005.
[26] Tasdemirci A, Hall IW. The effects of plastic deformation on stress wave propagation in multi-layer composite materials. Int J Impact Eng 2007;34(11):1797–813.
[27] Tasdemirci A, Hall IW, Gama BA, Guden M. Stress wave propagation effects in two- and three-layered composite materials. J Compos Mater 2004;38(12):995–1009.
[28] Brara A, Camborde F, Klepaczko JR, Mariotti C. Experimental and numerical study of concrete at high strain rates in tension. Mech Mater 2001;33(1):33–45.